both the hardware and software can hardly be considered a surprise. The equipment was conceived as experimental and was built only to show feasibility. Schedules did not allow complete testing, so that changes to the system were necessary while data collection was in progress.

The actual reject rate experienced by the subjects ranged from 2–6 percent on a weekly basis, deteriorating as hardware and file problems gradually ruined the references. The average online figure including all hardware and system problems was 4.9 percent. Nonetheless, it was interesting to observe that the prevailing opinion of the users was that the system worked well. There were, after all, about 100 sessions per day with a total of one to six rejects; thus the failures were not very frequent, fewer than 1/h. Most of these rejects were, we emphasize, due to implementation problems. The particular hardware problems were

a) baseline drift in the pressure channel, ruining the correlations;
b) digital noise in the pressure channel, making the signature appear longer;
c) lack of reset to serial number register, allowing accidental use of prior signer's number;
d) long term changes in characteristics of the pressure channel, probably caused by deterioration of the strain-gauge adhesive;
e) lack of interchangeable pen cartridges and truly identical pressure characteristics from pen to pen.

The redesign feature was needed for about 2 percent of the subjects. It is effective but could be improved by more stringent criteria. More than one success could be required to enroll a user, and an additional requirement that the successes be well-separated in time could be imposed, e.g., on different days.

The adaptation feature was designed to cope with slow changes in the hardware, drift, and temporary confusion over styles. We did not expect that some users would continually vary between two different signature styles. This could be guarded against administratively by issuing signature cards with an embossed reference signature. As it happened, only 3/248 users vacillated in this way, so the problem was not widespread. Use of the adaptation feature carelessly or during intervals of subtle hardware malfunction can destroy the reference file and degrade the performance, as we have seen.

In summary, our dynamic signature verification is capable of high performance in a realistic application. The performance shown during this test was superior to the published data on other techniques such as speaker identification and fingerprint scanning and comparable to the reject rates involving memorized code numbers (PIN's) which are far less secure. The signature technique is robust and general, but because of the relative ease of forging some signatures and the substantial human factors involved in establishing proper reference patterns, the system must be designed with care. Even higher performance levels are possible, but require that the signers be motivated to a greater extent than achieved in this experiment.

Acknowledgment

The authors particularly wish to thank J. Kurtzberg, who shared the burden of running the online experiment; T. Perry and B. Marinnello who were responsible for all the electronic hardware; and H. Pannissidi and C. Watters who designed and constructed the pens. G. Nikolsky, SMD Poughkeepsie, installed the strain gauges. We are also grateful to the many people in DP headquarters who made the test possible, including C. Aghina, D. Stavola, W. W. Jayne, and J. Ritchie. In addition, we wish to thank the operators in the I/O room for their cooperation, and above all, the 248 subjects who overcame their initial skepticism and graciously contributed their signatures.

Appendix

If the two orthogonal acceleration channels are labeled x and y and the sample and reference signals are

$$s(t) = \langle s_x(t),\ s_y(t),\ s_p(t)\rangle$$

$$r(t) = \langle r_x(t),\ r_y(t),\ r_p(t)\rangle.$$

Then for the ith segment, the correlations are defined as

$$C_a^i = \frac{\left|\max_\tau \sum_t [s_x^i(t) + js_y^i(t)][r_x^i(t+\tau) - jr_y^i(t+\tau)]\right|}{\left[\sum_t \{[s_x^i(t)]^2 + [s_y^i(t)]^2\} \sum_t \{[r_x^i(t)]^2 + [r_y^i(t)]^2\}\right]^{1/2}}$$

and

$$C_p^i = \frac{\max_\tau \sum_t [s_p^i(t)][r_p^i(t+\tau)]}{\left[\left\{\sum_t [s_p^i(t)]^2\right\}\left\{\sum_t [r_p^i(t)]^2\right\}\right]^{1/2}}.$$

Let n_i be the corresponding segment lengths of the reference signature. We define a verification measure V as

$$V = \sum_i \left(n_i / \sum_i n_i\right) C^i$$

where

$$C^i = [C_a^i + C_p^i]/2.$$

References

[1] N. M. Herbst and C. N. Liu, "Automatic signature verification based on accelerometry," *IBM J. Res. and Devel.*, vol. 21, pp. 245–253, May 1977.
[2] ——, "Automatic verification of signatures by means of acceleration patterns," *Proc. IEEE Comp. Soc. Conf. On Pattern Recognition and Image Processing*, Troy, NY, June 1977, pp. 331–336.
[3] ——, "Automatic signature verification," *IBM Research Rep.*, RC-5810, Nov. 1975.
[4] J. Sternberg, "Automatic signature verification using handwriting pressure," *1975 Wescon Tech Papers*, Paper No. 31/4, Los Angeles, Sept. 1975.
[5] H. D. Crane, D. E. Wolf, and J. S. Ostrem, "The SRI pen system for automatic signature verification," *Symp. Proc. NBS Trends and Applications 1977*, Gaithersburg, May 1977, pp. 32–39.
[6] A. Fejfar and J. Myers, "The testing of three automatic identity verification techniques for entry control," *Proc. 1977 Int. Conf. on Crime Countermeasures*, Oxford, July 1977.

Histogram Modification for Threshold Selection

JOAN S. WESZKA AND AZRIEL ROSENFELD, FELLOW, IEEE

***Abstract*—A standard approach to threshold selection for image segmentation is based on locating valleys in the image's gray-level histogram. Several methods have been proposed that produce a transformed histogram in which the valley is deeper, or is converted**

Manuscript received June 1, 1978; revised August 31, 1978. This work was supported by the Directorate of Mathematical and Information Sciences, U.S. Office of Scientific Research, under Grant AFOSR-77-3271.

J. S. Weszka was with the Computer Science Center, University of Maryland, College Park, MD 20742. She is now with the IBM Corporation, Austin, TX 78759.
A. Rosenfeld is with the Computer Science Center, University of Maryland, College Park, MD 20742.

into a peak, and is thus easier to detect. The transformed histograms used in these methods can all be obtained by creating (gray level, edge value) scatter plots, and computing various weighted projections of these plots on the gray-level axis. Using this unified approach makes it easier to understand how the methods work and to predict when a particular method is likely to be effective. The methods are applied to a set of examples involving both real and synthetic images, and the characteristics of the resulting transformed histograms are discussed.

I. Introduction

Many types of images contain dark objects on a light background, or vice versa—for example, printed characters on paper, chromosomes on a microscope slide, or clouds above the sea surface. Such images can be segmented into objects and background by thresholding—i.e., by assigning each image pixel to one of two classes, light and dark, according to whether its gray level is lighter or darker than a specified threshold t. For a discussion of thresholding see [1].

Thresholding is a special case of pattern classification in which a one-dimensional feature space is used, the feature being the gray level of the pixel. The threshold is a "hyper-plane" decision surface (i.e., a point) in this one-dimensional space. If we knew the distribution of gray levels in the given ensemble of images—e.g., if we knew that the gray levels were a mixture of two Gaussian populations with given means and standard deviations—then we could determine analytically the threshold that minimizes the classification error. In the absence of such knowledge, we can approach the problem of threshold selection by performing cluster analysis on the feature space. Suppose that we construct the gray-level histogram of the image (or ensemble); this is a plot showing how often each gray level occurs. A cluster of feature values is then nothing more than a peak on the histogram, corresponding to a densely populated range of gray levels. If we find two peaks on the histogram, it is reasonable to choose a threshold that separates these peaks, e.g., at the bottom of the valley between them, since this threshold appears to separate the gray-level population into two distinctive subpopulations. Similarly, if there are three or more peaks, we can segment the image using two or more thresholds at the intervening valley bottoms. This method of threshold selection was first described in [2].

Several methods have been proposed that produce a transformed gray-level histogram in which the valley is deeper, or is converted into a peak, and is thus easier to detect. The transformed histograms used in these methods can all be obtained by creating a (gray level, edge value) scatter plot for the given image (ensemble) and computing various weighted projections of this plot onto the gray-level axis. Using this unified approach makes it easier to understand how the methods work and to predict when a particular method is likely to be effective.

In Section II of this correspondence, we define the class of images to which these methods should be applicable. Section III describes the methods of producing transformed histograms, and Section IV shows how these methods all reduce to constructing weighted projections of (gray level, edge value) scatter plots. In Section V and VI, the methods are applied to a set of examples involving both real and synthetic images, and the characteristics of the resulting transformed histograms are discussed.

II. The Underlying Image Model

We shall assume that the given images consist of objects on a background, where the objects and background each have a unimodal gray-level population. We further assume that the gray levels of adjacent points interior to the objects, or to the background, are highly correlated, while across the edges at which objects and background meet, adjacent points differ significantly in gray level.

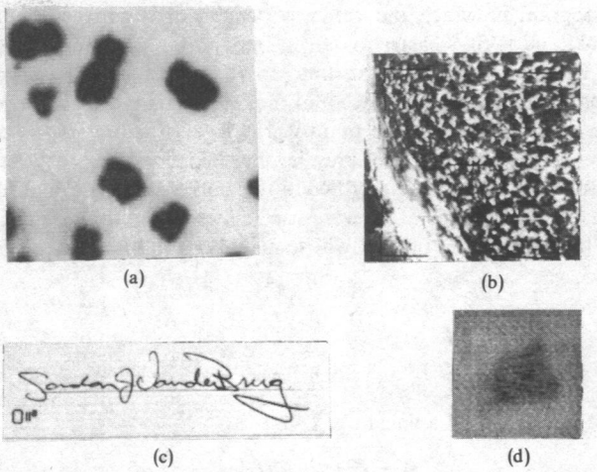

Fig. 1. Test images: (a) chromosomes, (b) cloud cover, (c) handwriting, (d) tank.

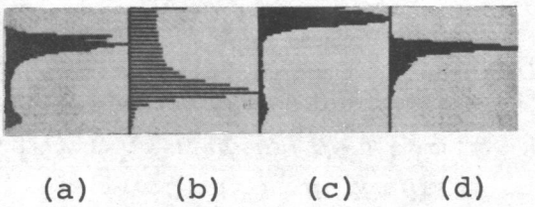

Fig. 2. Histograms of images in Fig. 1.

If an image satisfies these assumptions, its gray-level histogram will be primarily a mixture of two unimodal histograms corresponding to the object and background populations, respectively. If the means of these populations are sufficiently far apart, their standard deviations are sufficiently small, and they are comparable in size, the image histogram will be bimodal. Otherwise, the histogram may be unimodal, but one side of the peak may display a shoulder or slope change, or one side may be less steep than the other, reflecting the presence of two peaks that are close together or that differ greatly in height. The histogram will also contain a third, usually smaller, population corresponding to points on the object/background border (since this is not perfectly sharp, in general). These points have gray levels intermediate between those of the object and background; their presence raises the level of the valley floor between the two peaks, or if the peaks are already close together, makes it harder to detect the fact that they are not a single peak.

Four images that appear to satisfy these assumptions are shown in Fig. 1. Part (a) of this figure is a photomicrograph of some chromosomes; part (b) is a television image of cloud cover as seen by a meteorological satellite; part (c) is a signature on a bank check; and part (d) is an infrared image of a tank against a terrain background. The histograms of these four images are shown in Fig. 2. (In the case of part (b), the image contained only even-numbered gray levels, so that the histogram bars are spread apart.)

III. Methods of Producing Transformed Histograms

If the histogram peaks are close together or very unequal in size, it may be difficult to detect the valley between them. This section describes several methods of producing a transformed

histogram in which the valley is deeper, or is converted into a peak, and is thus easier to detect. In determining how each point of the image should contribute to the transformed histogram, these methods take into account the rate of change of gray level at the point, as well as the point's gray level. For brevity, we shall refer to rate of change of gray level as "edge value."

In the experiments described in this correspondence, five different edge-value operators were used. These operators are defined as follows, for the pixel E whose neighborhood is

$$\begin{array}{cccc} A & B & C & \\ D & E & F & G \\ H & I & J & K \\ & L & M & \end{array}$$

1) LAP, the "Laplacian":

$$\left| E - \frac{A+B+C+D+F+H+I+J}{8} \right|,$$

2) ROB, the "Roberts cross":

$$\max\left[|E-C|, |B-F|\right],$$

3) DIF1, the max of differences of average gray levels in pairs of horizontally and vertically adjacent 2-by-2 neighborhoods:

$$\tfrac{1}{4}\max\left[|B+C+E+F-I-J-L-M|,\right.$$
$$\left.|D+E+H+I-F-G-J-K|\right],$$

4) DIF2, analogous to DIF1 but using pairs of 4-by-4 neighborhoods,
5) DIF3, analogous but using 8-by-8 neighborhoods.

A. Histogram of Points Having Low Edge Values

According to the image model described in Section II, points interior to the objects and background should generally have low edge values, since they are highly correlated with their neighbors, while those on the object/background border should have high edge values. Thus if we produce a histogram of the gray levels of points having low edge values only, the peaks should remain essentially the same, since they correspond to interior points, but the valley should become deeper, since the intermediate-gray-level points on the object/background border have been eliminated. (See Panda and Rosenfeld [3].)

More generally, we can compute a weighted histogram in which points having low edge values are counted heavily, while points having high edge values are counted less heavily. For example, if $|\Delta|$ is the edge value at a given point, one could give that point weight $1/(1+|\Delta|^2)$ in the histogram; this gives full weight (1) to points having zero edge value and negligible weight to high edge value points. This method was proposed by Mason *et al.* [4] and has also been investigated by Weszka and Rosenfeld [5].

B. Histogram of Points Having High Edge Values

Conversely, suppose that we produce a histogram of the gray levels of only those points that have high edge values. If edge values are high at the object/background border and low elsewhere, the resulting histogram should have a single peak at a value intermediate between the object and background gray levels. Thus the mode of this histogram, or perhaps its mean, should be a good threshold. This method was first suggested by Katz [6] and has also been studied by Weszka and Rosenfeld [7].

An alternative possibility arises if we use the absolute-value Laplacian operator

$$\left| \frac{\partial^2 f}{\partial x^2} + \frac{\partial^2 f}{\partial y^2} \right|$$

or its finite-difference analog

$$|\Delta_x^2 f + \Delta_y^2 f|$$

to define "edge value." Since these are second-derivative operators, they have value zero on a linear ramp, but high values on the shoulders at the top and bottom of a ramp. Thus if the object/background borders are ramplike, the points having high Laplacian values will be adjacent to, but not on, these borders. The histogram of high Laplacian-value points should thus have two peaks, representing object and background gray levels, but the valley between these peaks should be quite deep, since the Laplacian has low values at the intermediate-gray-level points that lie on the borders. Moreover, the peaks should be relatively equal in size, since the border zones in the objects and the background should have comparable areas, even if the objects and background themselves have very different areas. This method was introduced by Weszka *et al.* [8].

More generally, we can compute a weighted histogram in which points having high edge values are counted more heavily than those having low edge values. For example, we can give each point its edge value $|\Delta|$ as a weight, so that zero edge value points are not counted at all, while high edge value points are counted heavily. This method, which was proposed by Watanabe [9], is equivalent to summing the edge values for each gray level. If the edge values at the object/background borders are very high, the resulting histogram will have a peak at a gray level intermediate between those of object and background, and this peak can be used as a threshold. However, a possible difficulty with this method is that if the areas of the objects and background are large, the sum of the large numbers of low edge values in their interiors may be higher than the sum of the smaller number of high edge values at the borders, and the peak may not exist. To avoid this objection, Weszka *et al.* [10] proposed using the average, rather than the sum, of the edge values for each gray level; this average should certainly be higher for the border gray levels than it is for the interior gray levels.

IV. (Gray Level, Edge Value) Scatter Plots

Scatter plots of gray level versus edge value for the images of Fig. 1 are shown in Fig. 3. In these plots, the origin is in the upper left corner; gray level increases to the right, and edge value increases downward.[1] The darkness of a point on these plots is proportional to the log of the number of times that the corresponding pair of (gray level, edge value) values occurs; log scaling was used to make faint clusters more easily visible.

All of the transformed histograms described in Section III can be obtained by constructing a two-dimensional scatter plot of gray level versus edge value for the given image (or ensemble) and computing various weighted projections of this plot onto the gray-level axis. In pattern classification terms, this can be thought of as first plotting the image pixels in a two-dimensional feature space and then transforming the space back to one dimension to obtain the new histogram.[2]

Specifically, when we produce a histogram of the gray levels of the low edge value points only, we are in effect applying a steplike weighting function to the scatter plot, giving weight 1 to low edge values and weight 0 to high edge values. In the method of Mason

[1] For technical reasons, it was not possible to orient the histograms (Figs. 2, 4–8, 10, 12–16) consistently with the scatter diagrams (Figs. 3, 11); in the former, gray level increases downward.

[2] Some other methods of using the (gray level, edge value) feature space to classify pixels (and thus to segment the image) are described in [3]. Watanabe (personal communication) has also used scatter plots of gray level versus cumulative edge value for image segmentation.

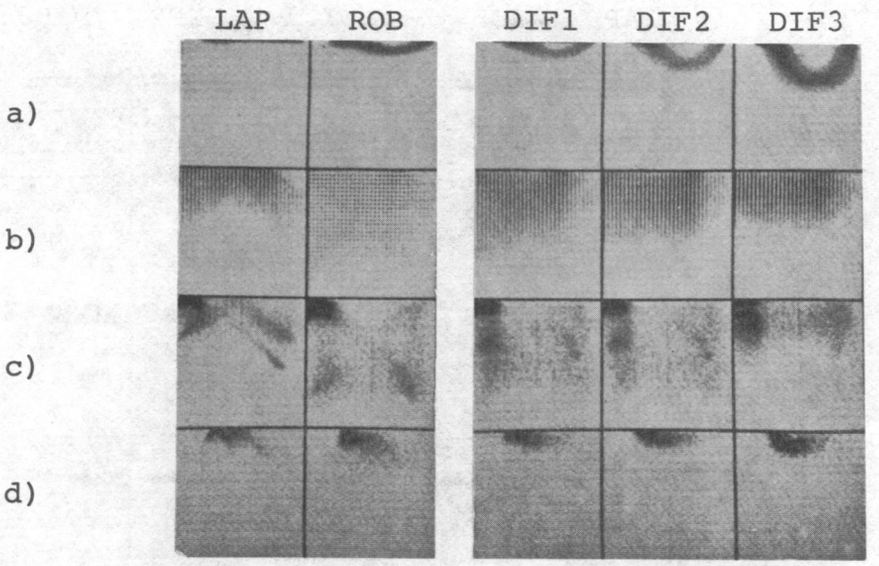

Fig. 3. Scatter plots of gray level versus edge value for images of Fig. 1, using edge-value operators LAP, ROB, DIF1, DIF2, and DIF3 (see text).

et al., we are applying the weighting function $1/(1 + |\Delta|^2)$, where $|\Delta|$ is the edge value. In Katz's method, we are again using a step function, but with high edge values having weight 1 and low values weight 0; similarly for the method of Weszka *et al.*, but using the Laplacian as an edge value. Finally, in Watanabe's method we are using $|\Delta|$ as a weighting function; while in the modification of this method by Weszka *et al.*, we are pointwise dividing Watanabe's weighted histogram by the original unweighted histogram.

We can understand more readily how the methods of Section III work, and when they are likely to be effective, by considering what the (gray level, edge value) scatter plot can be expected to look like for images that satisfy the assumptions made in Section II. On such a plot, there should be two large clusters of points near the gray-level axis, representing pixels interior to the objects and background, which should have low edge values. The shapes of these clusters will depend on the degree to which the interior points are correlated. If the correlation is very high or if the edge operator is not too sensitive to noise, these clusters should be compact and should lie close to the gray-level axis. On the other hand, if the correlation is lower or the edge operator is noise-sensitive (the Laplacian, for example), we can expect the clusters to extend farther from the axis at the ends of the (object or background) gray-level range, since these gray levels will be rarer and so are more likely to be associated with high edge values.

There should also be points on the plot corresponding to object/background border points, but the location of these points depends on the sharpness of the borders and on the nature of the operator used to define edge value. For example, if the borders are ramplike and a first-derivative edge operator such as the gradient magnitude is used, there should be a cluster of border points joining the object and background clusters. This border cluster should extend away from the gray-level axis by an amount that depends on the maximum steepness of the borders. If a Laplacian operator is used, the border points should not give rise to intermediate-level points that extend away from the axis.[3]

[3] This description assumes that the objects and background have relatively large interiors, and do not consist primarily of border points. For the signature image (Fig. 1(c)), this is not the case; the object points are virtually all border points. The images of Fig. 1 will be discussed further in the next section.

V. Examples

(Gray level, edge value) scatter plots for the images of Fig. 1 were shown in Fig. 3. We can make the following comments on these scatter plots.

a) In the chromosome image, the objects and background are quite smooth, so that the object and background clusters are close to the gray-level axis. In addition, the border ramps are shallow; thus the edge operators having small sets of support (ROB, DIF1) do not give rise to points far from the gray-level axis. This is true even for the Laplacian operator, since the chromosome image is highly correlated and noise-free. For the larger operators, on the other hand, the maximum edge value approaches the contrast between the objects and the background and is much farther from the axis.

b) In the cloud image, the objects and background are noisy, so that the scatter plots are spread far from the gray-level axis when small-support edge operators that respond to the noise are used, but they are concentrated closer to the axis when larger operators are used. For the Laplacian operator, there is a slight tendency for the rarer gray levels to yield higher Laplacian values.

c) In the signature image, as mentioned earlier, virtually all the object points are border points. Thus for the small-support edge operators, the "object" cluster is far from the gray-level axis, and the background cluster also extends far from the axis due to the high contrast between objects and background. For the larger operators, on the other hand, the object/background contrast decreases, since the neighborhoods used in these operators can never be contained inside the objects; thus the clusters move closer to the axis as the operator size increases. The tendency for rarer gray levels to have higher edge values is noticeable for the small operators in the background cluster and strongly present in the object cluster.

d) The scatter plots for the tank image generally resemble those of the chromosome image, allowing for the fact that the tank image has lower contrast and is somewhat noisier. In particular, the rare gray level/high edge value trend is quite noticeable for the Laplacian operator.

Based on these descriptions of the scatter plots, we can judge how the methods of Section III might be expected to work for the four images.

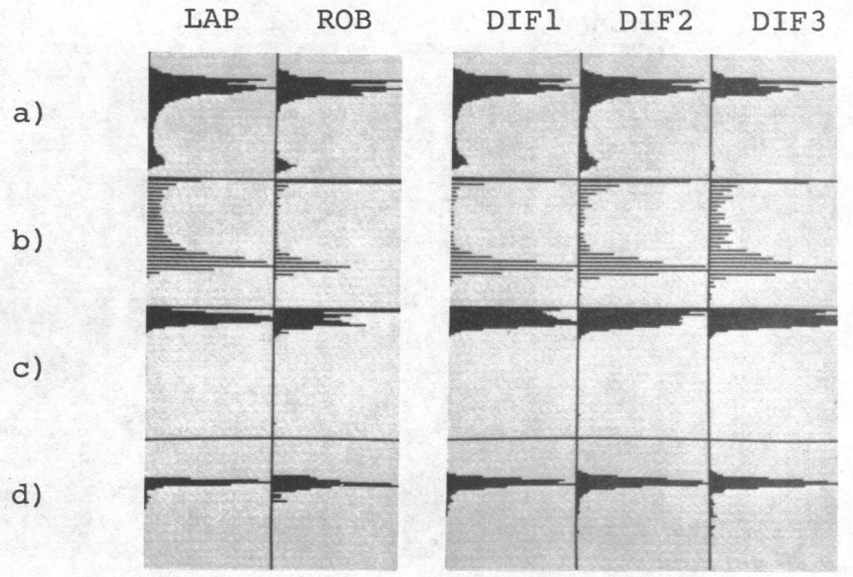

Fig. 4. Histograms of gray levels of zero edge value points for four images.

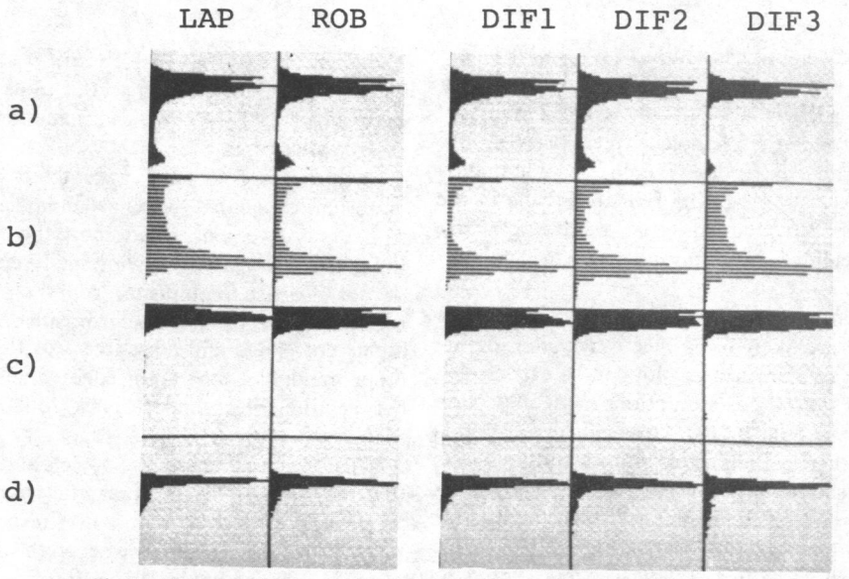

Fig. 5. Histograms for four images in which points having low edge values are given higher weights.

1) The results using Panda's method, histograms of the points having edge value zero only, are shown in Fig. 4. As expected, for the chromosome and tank images, the valley deepening effect is greatest for the operators having large sets of support, while the reverse is true for the cloud image. The method fails for the signature image, where the objects contain almost no zero edge value points, since they have no interiors. It also fails for the Laplacian operator in all cases, since the intermediate gray levels are not expected to have high Laplacian values, so that restricting the histogram to low Laplacian values is not expected to have a valley-deepening effect. Analogous remarks apply to Mason's method, as seen in Fig. 5.

2) Results using Katz's method here are shown in Fig. 6, with high edge values defined using four different percentiles: 80, 85, 90, and 95 percent. (For some of these, no histograms are shown because the percentile was reached for zero edge value, so that the method yielded the same result as Panda's.) As expected, for the chromosome and tank images, unimodal histograms are usually obtained, especially for the higher percentiles. The cloud image also tends to yield unimodal histograms, but the position of the mode is less reliable, owing to the high variability of the edge values for this image. The signature image does not yield unimodal histograms, which is also as expected, since its border point population contains its object point population.

3) The method of Weszka *et al.* (see Fig. 7), based on points having high Laplacian values, does produce a slight valley deepening for the chromosome image, but its effect is small since this image has almost no points with high Laplacian values. For the other three images, the method gives rise to a pair of relatively equal peaks, particularly for the highest percentiles. However, inspection of the scatter plots suggests that these peaks correspond to the high Laplacian values at rare (= high or low) gray levels, rather than representing high Laplacian values adjacent to object/background borders. The method produces histograms

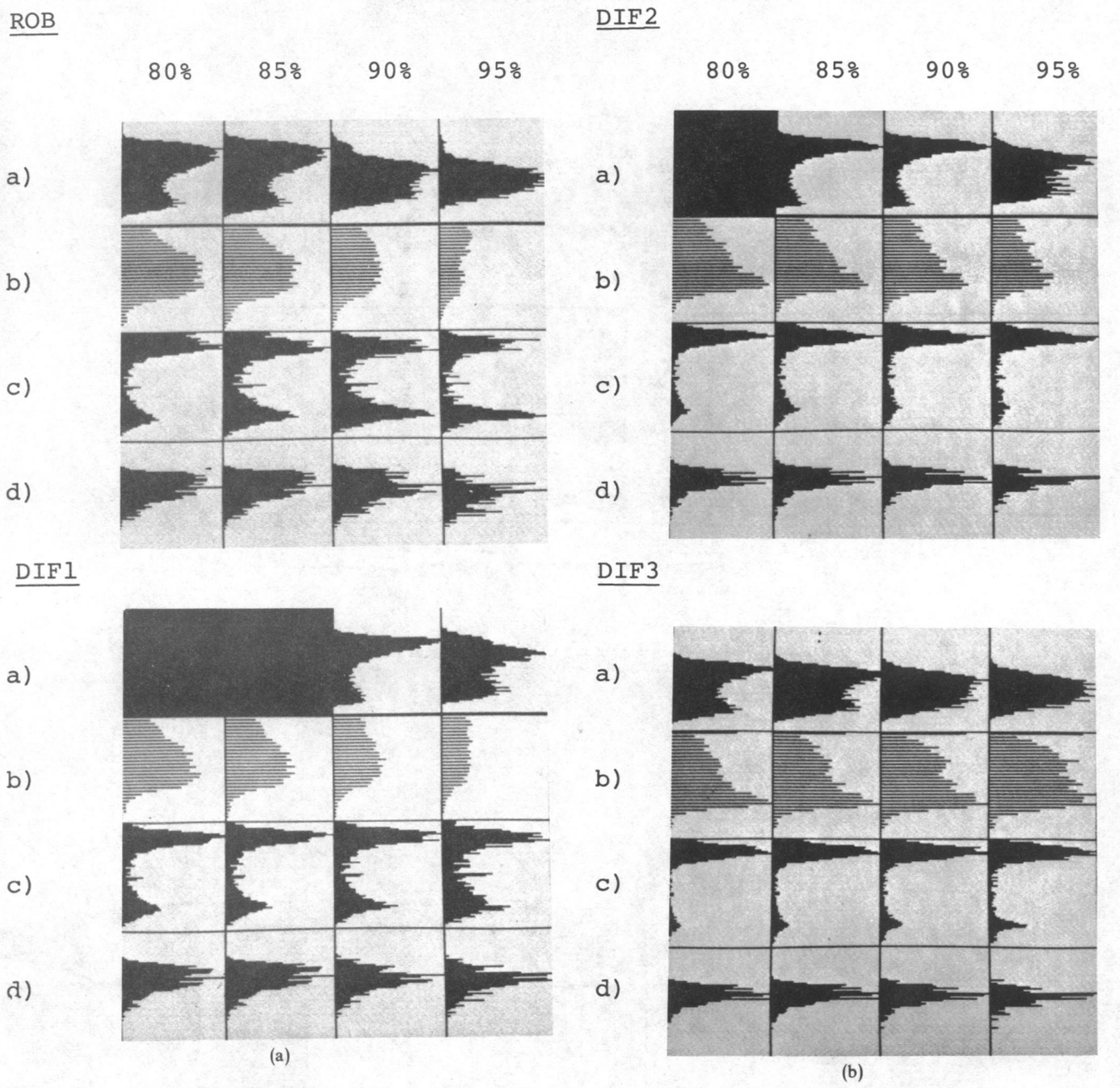

Fig. 6. Histograms of gray levels of high edge value points (percentiles 80, 95, 90, 95) for four images using four gradient operators.

whose valleys yield reasonable thresholds, but this may simply be because any threshold intermediate between the high and low gray levels would be reasonable for these images.

4) Watanabe's method fails for all four images, for both the gradient and Laplacian operators, as shown in Fig. 8. As pointed out in Section III, the background points continue to dominate the histogram, since there are so many more of them, even though the border points have higher edge values. Weszka's modification of this method, for the gradient operators, is more successful if we ignore the high values at the ends of the gray-level range (which result from dividing by very low values on the original histogram).

VI. Synthetic Examples

In order to further study the dependence of the scatter plots on the statistics of the image regions, a set of synthetic images was generated. Each of these images, shown in Fig. 9, contains a square "object" region (amounting to about 10 percent of its area) having mean gray level 40 (on a 0–63 gray scale) and a background region having mean gray level 20. The gray levels of the object and background have approximately Gaussian distributions (truncated at 0 and 63) with standard deviation 7 in the object regions, and 3 (Figs. 9(a), (d), (g)), 5 (Figs. 9(b), (e), (h)), or 7 (Figs. 9(c), (f), (i)) in the background region. In Fig. 9(a)–(c), the gray levels of neighboring points are uncorrelated. The remaining parts of Fig. 9 were obtained by starting with uncorrelated gray levels and introducing correlation by local averaging, using neighborhood sizes 2×2 (Fig. 9(d)–(f)) and 4×4 (Fig. 9(g)–(i)), respectively. (To compensate for the fact that averaging reduces the standard deviation, larger standard deviations (6, 10, 14, 12, 20, 28) were used in the initial uncorrelated images; a larger gray-level range was used to accommodate Gaussian distributions with these large σ's.]

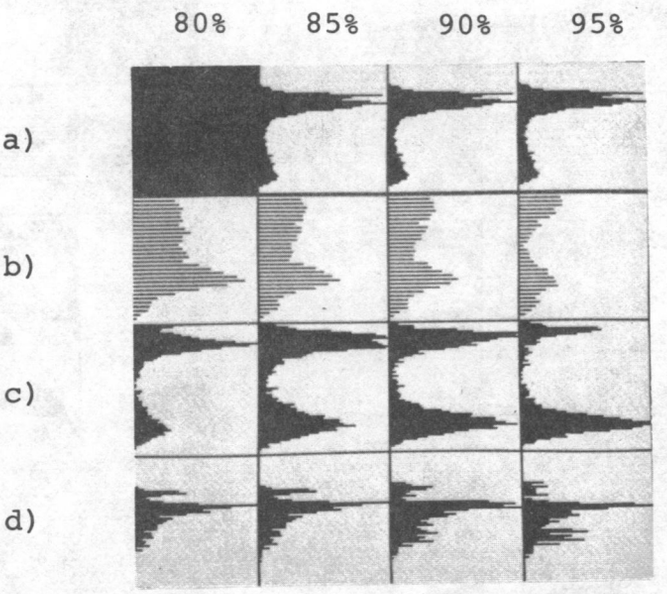

Fig. 7. Histograms of gray levels of high Laplacian-value points (percentiles 80, 85, 90, 95) for four images.

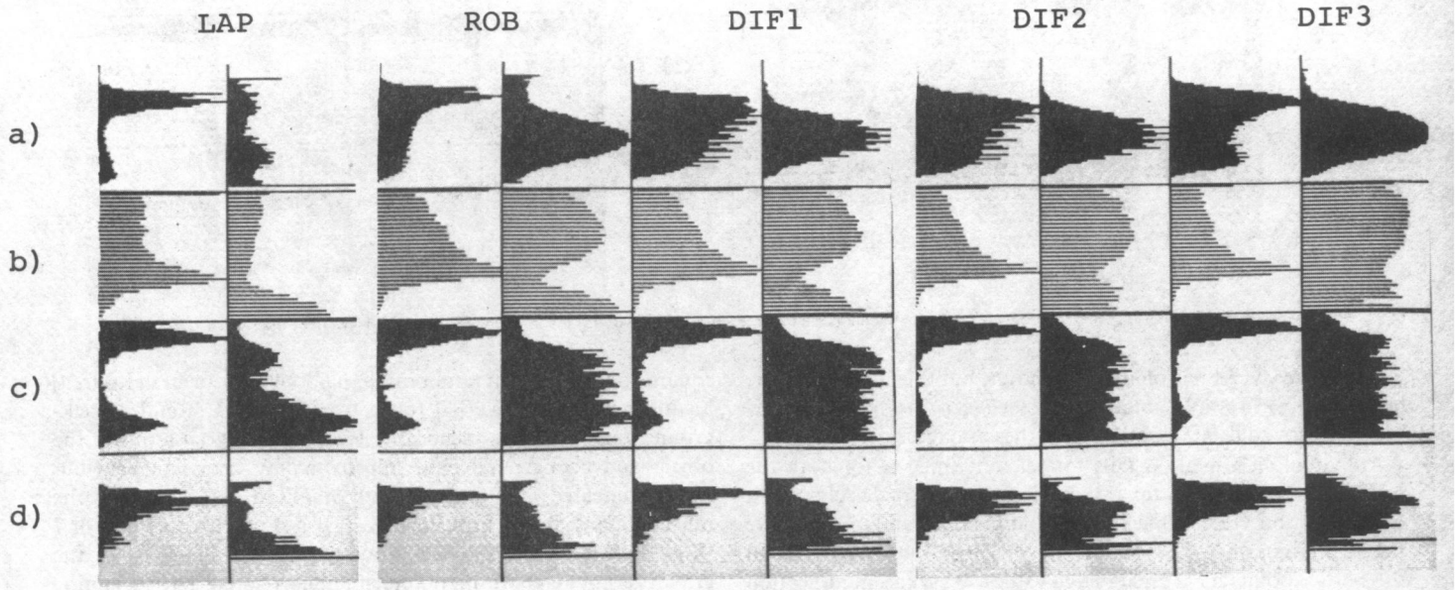

Fig. 8. Histograms for four images in which points having high edge values are given higher weights, and results of dividing these histograms pointwise by unweighted histograms.

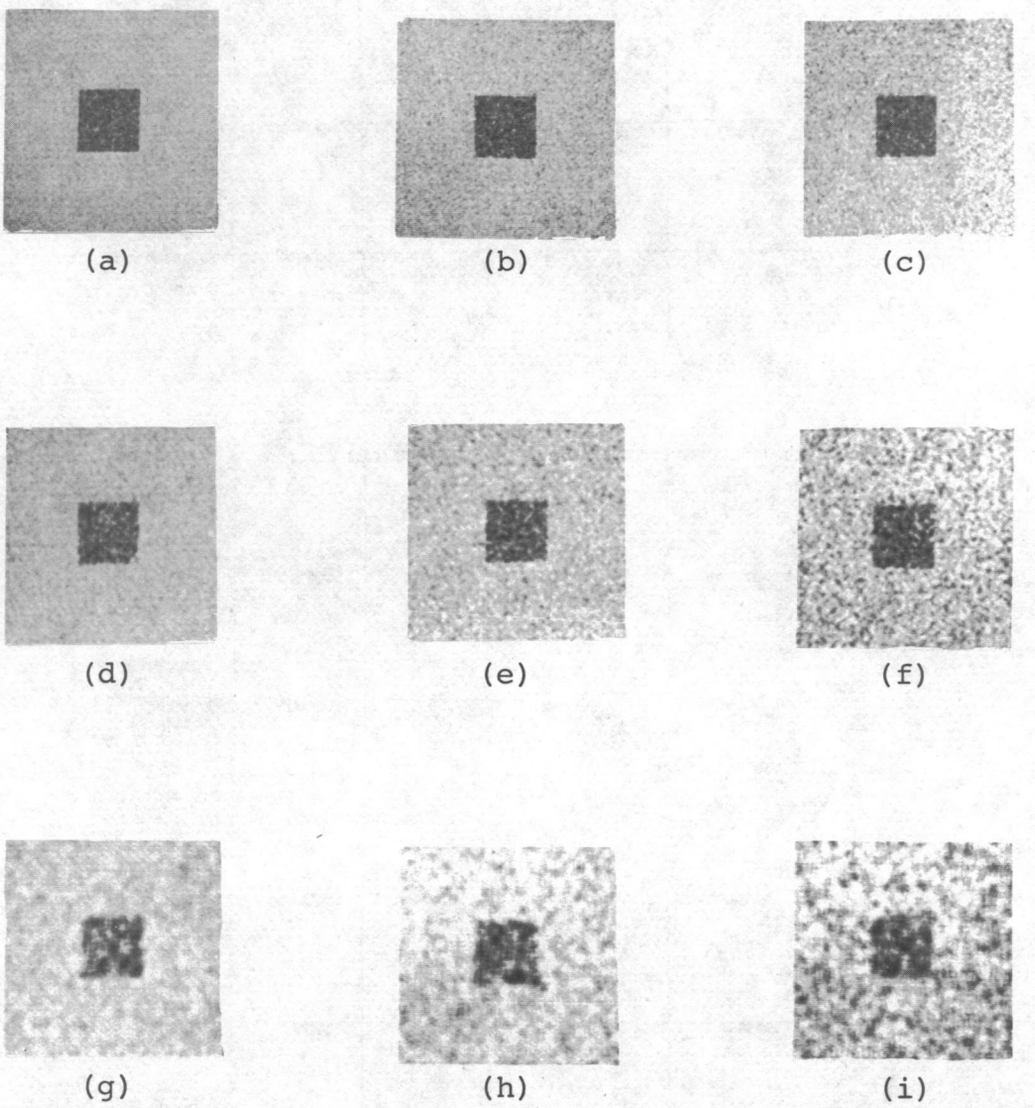

Fig. 9. Synthetic images: mean gray levels 20 (background) and 40 (object). Standard deviation of object gray levels 7; of background gray levels 3 (parts (a), (d), (g)), 5 (parts (b), (e), (h)), or 7 (parts (c), (f), (i)). In parts (a)–(c), no local averaging was done; in parts (d)–(f) and (g)–(i), local averaging was performed using 2×2 and 4×4 neighborhoods, respectively.

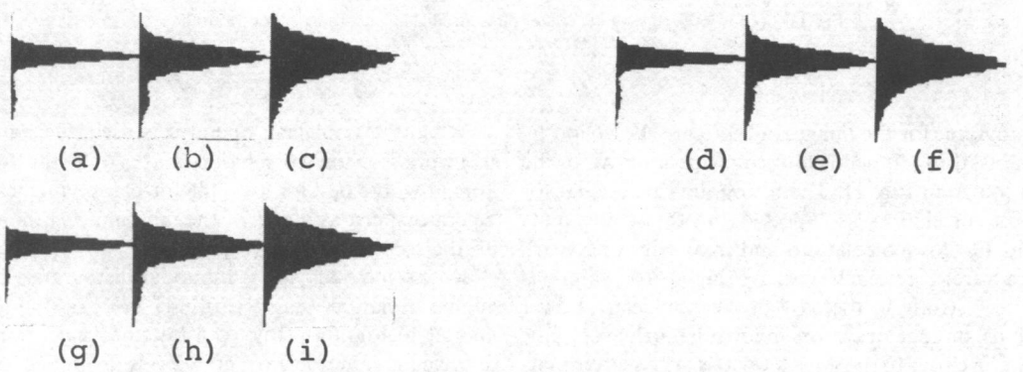

Fig. 10. Gray-level histograms for nine images in Fig. 9.

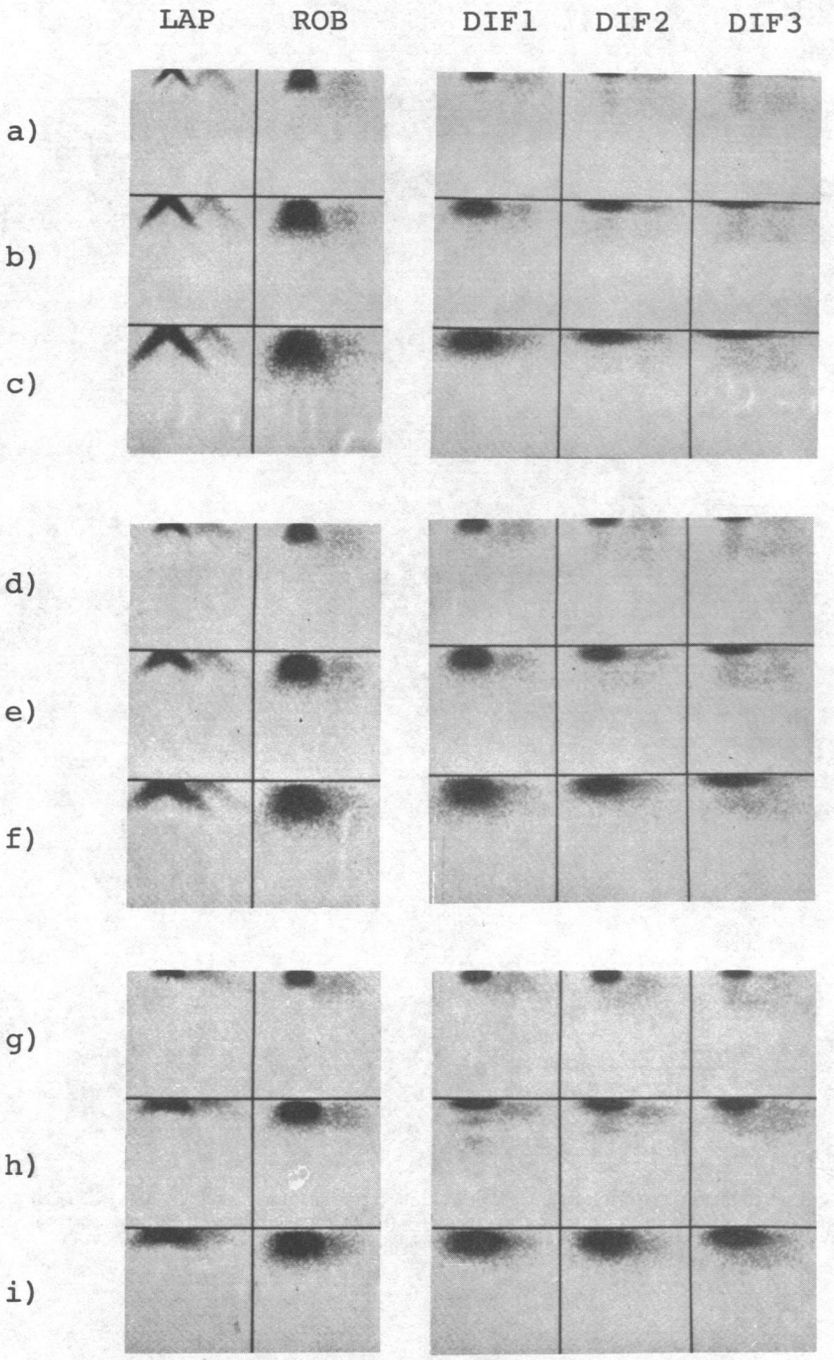

Fig. 11. (Gray level, edge value) scatter plots for nine images, using edge operators LAP, ROB, DIF1, DIF2, DIF3.

Gray-level histograms for the images in Fig. 9 are shown in Fig. 10, and scatter plots, using the same four edge operators as for the real images, are shown in Fig. 11. The histograms are similar for all four degrees of correlation, as expected, but the scatter plots differ appreciably. For low correlations and small edge operators, the tendency for rare gray levels to have high edge values is evident; this is very strong in the case of the Laplacian. Lower standard deviations, or edge operators involving much averaging, yield clusters that lie closer to the gray-level axis. The scatter plots for high correlation resemble those for the tank image.

When the Laplacian operator is used, the Panda method (Fig. 12) works for low-correlation images only; for the gradient operators, it works best for the high-correlation images using large edge operators, just as it did for the tank image. Similar remarks apply to the Mason method (Fig. 13).

Katz's method yields unimodal histograms, especially for the high-correlation images (Fig. 14). Weszka's method yields multimodal histograms (Fig. 15), but the peaks correspond to high Laplacian values at rare gray levels, as in Section V.

Watanabe's method does not yield useful central peaks for any

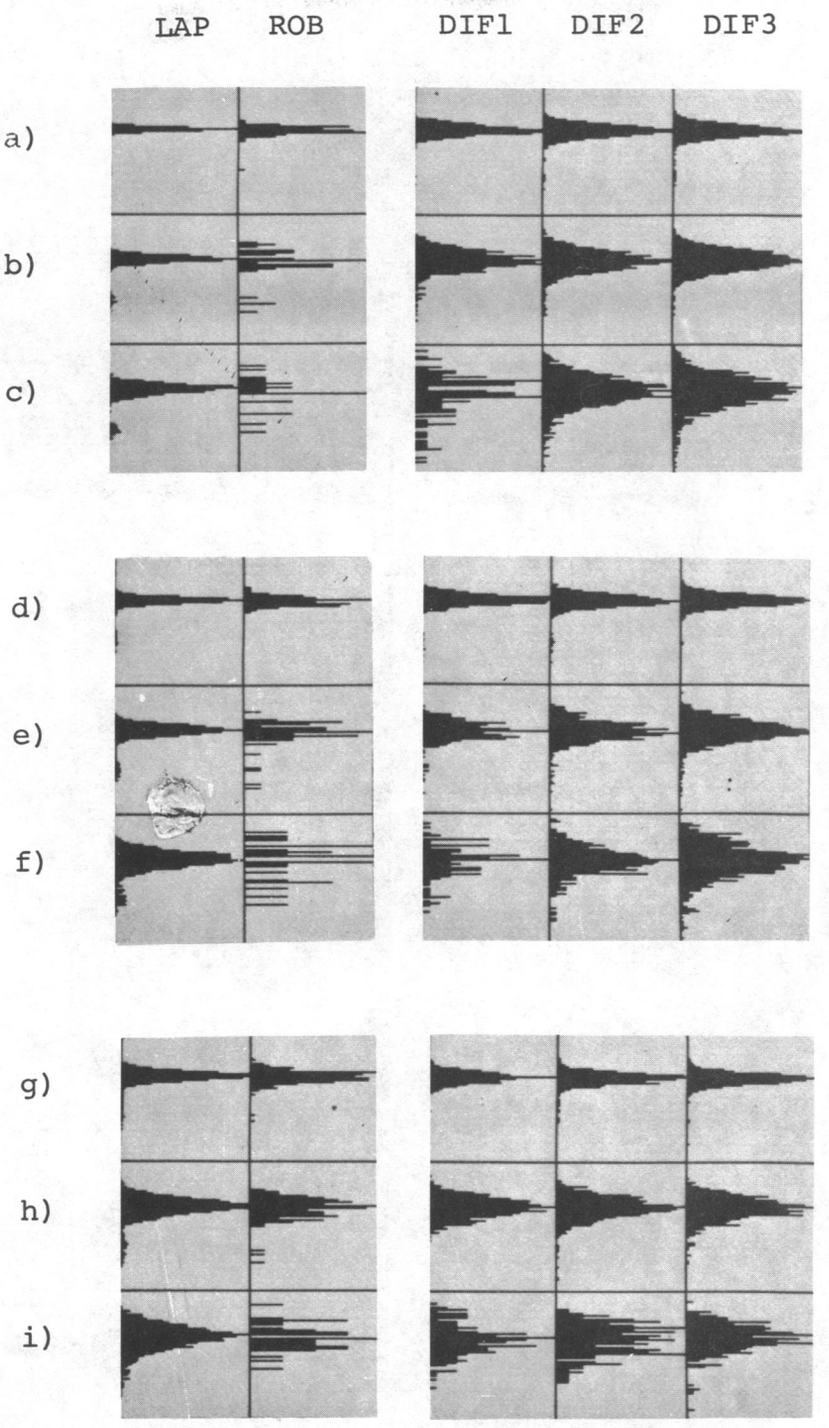

Fig. 12. Histograms of gray levels of zero edge value points for nine images.

of the operators. Weszka's modification does yield such peaks for the Laplacian operators and tends to do so for the gradient operators, particularly for the lower background standard deviations (Fig. 16).

VII. Concluding Remarks

The structure of the (gray level, edge value) scatter plots is influenced by several factors, including the smoothness of the image and the correlation of neighboring gray levels. Thus general criteria for predicting the degree to which a given method can be expected to work are not simple to formulate. However, as we have seen, examination of the scatter plot makes it easy to determine which methods will work for a given class of images. These scatter plots thus appear to be a useful tool for image analysis. Quantitative modeling of their structure (e.g., in terms of mixtures of two-dimensional distributions) would be desirable as a further aid to analyzing threshold selection techniques.

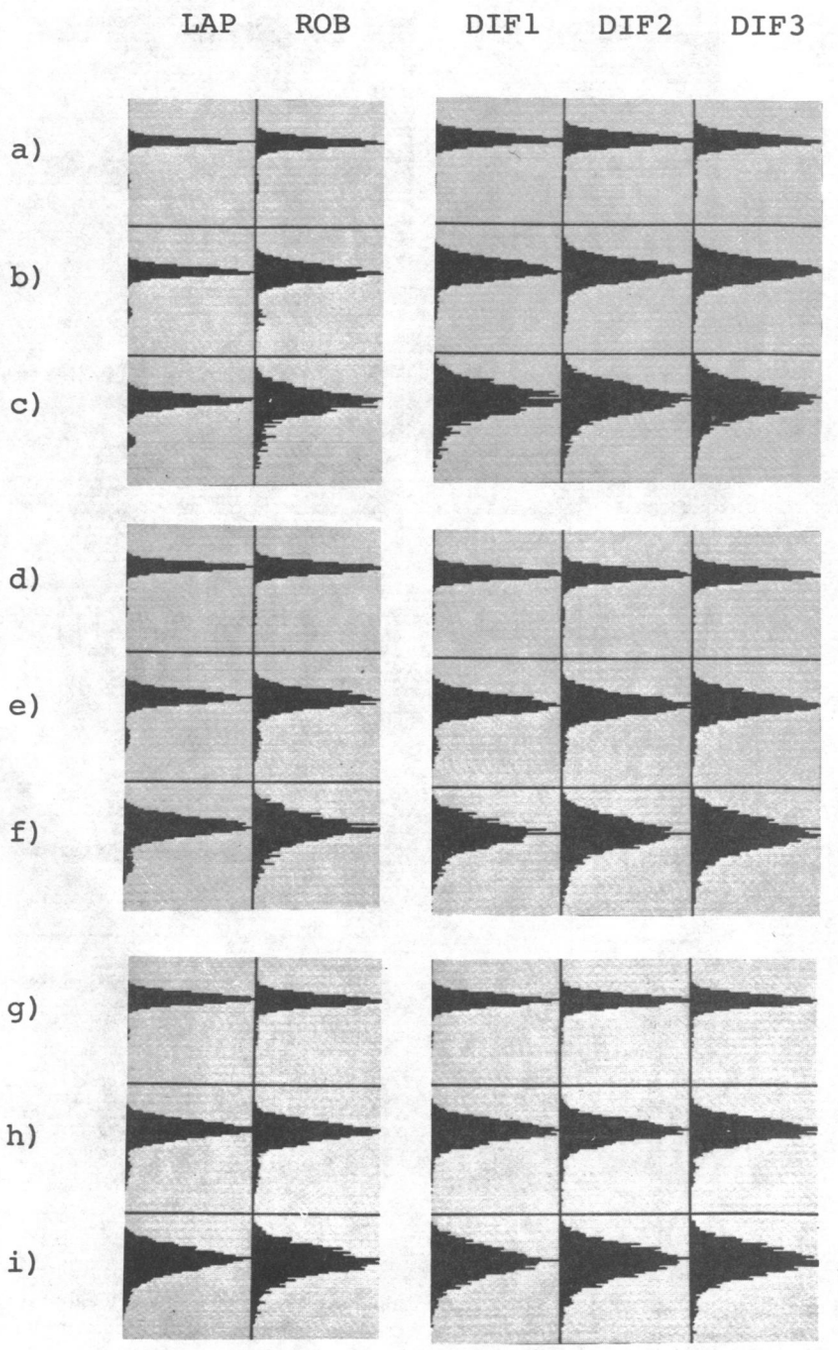

Fig. 13. Histograms for nine images in which points having low edge values are given higher weights.

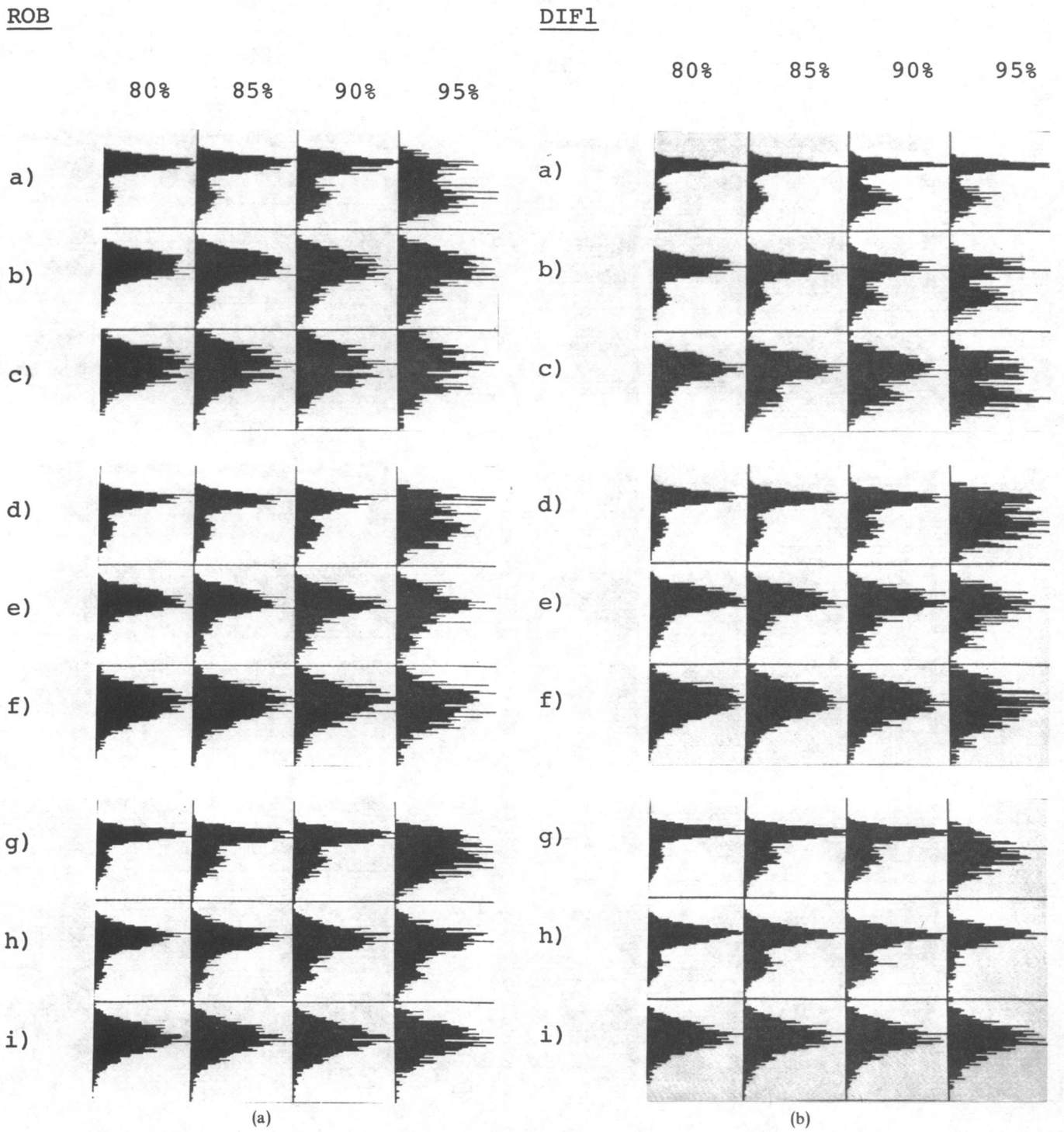

Fig. 14. Histograms of gray levels of high edge value points (percentiles 80, 85, 90, 95) for nine images, using four gradient operators.

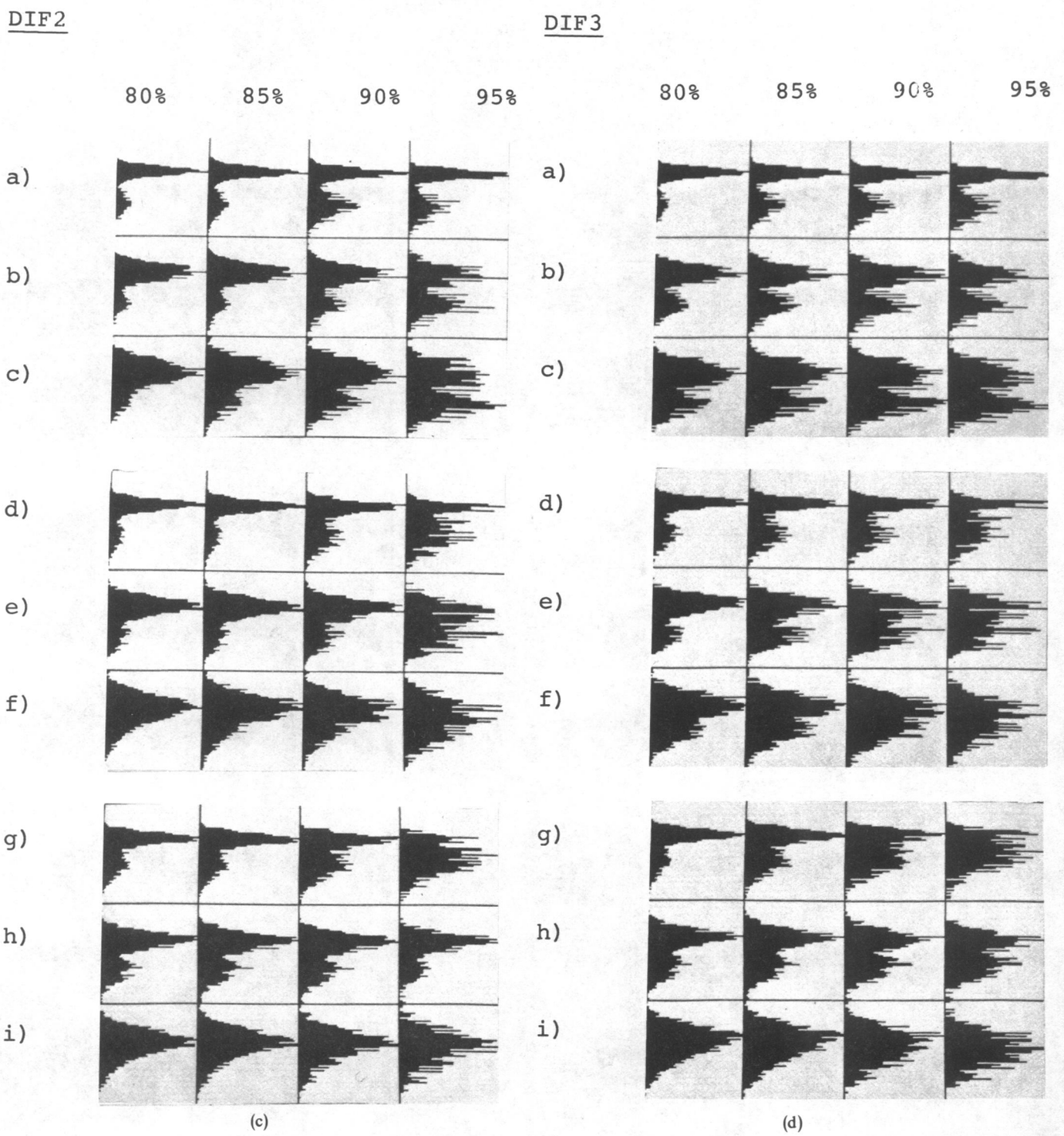

Fig. 14 (*Continued*)

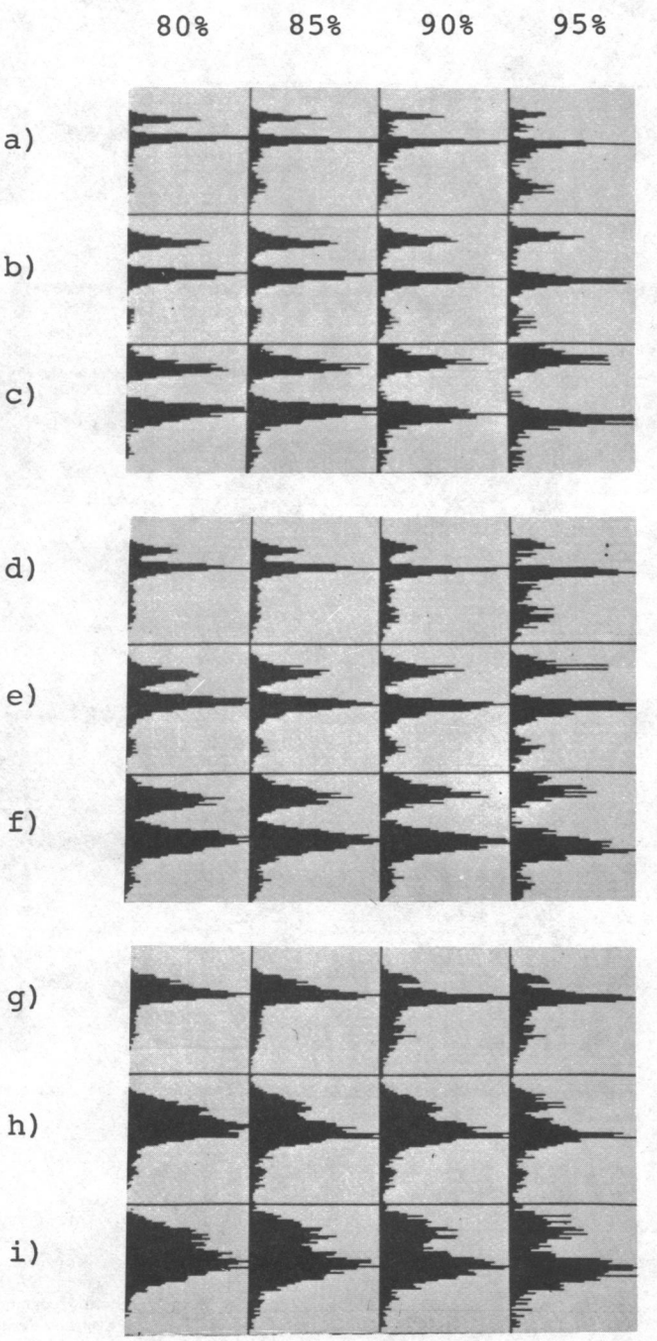

Fig. 15. Histograms of gray levels of high Laplacian value points (percentiles 80, 85, 90, 95) for nine images.

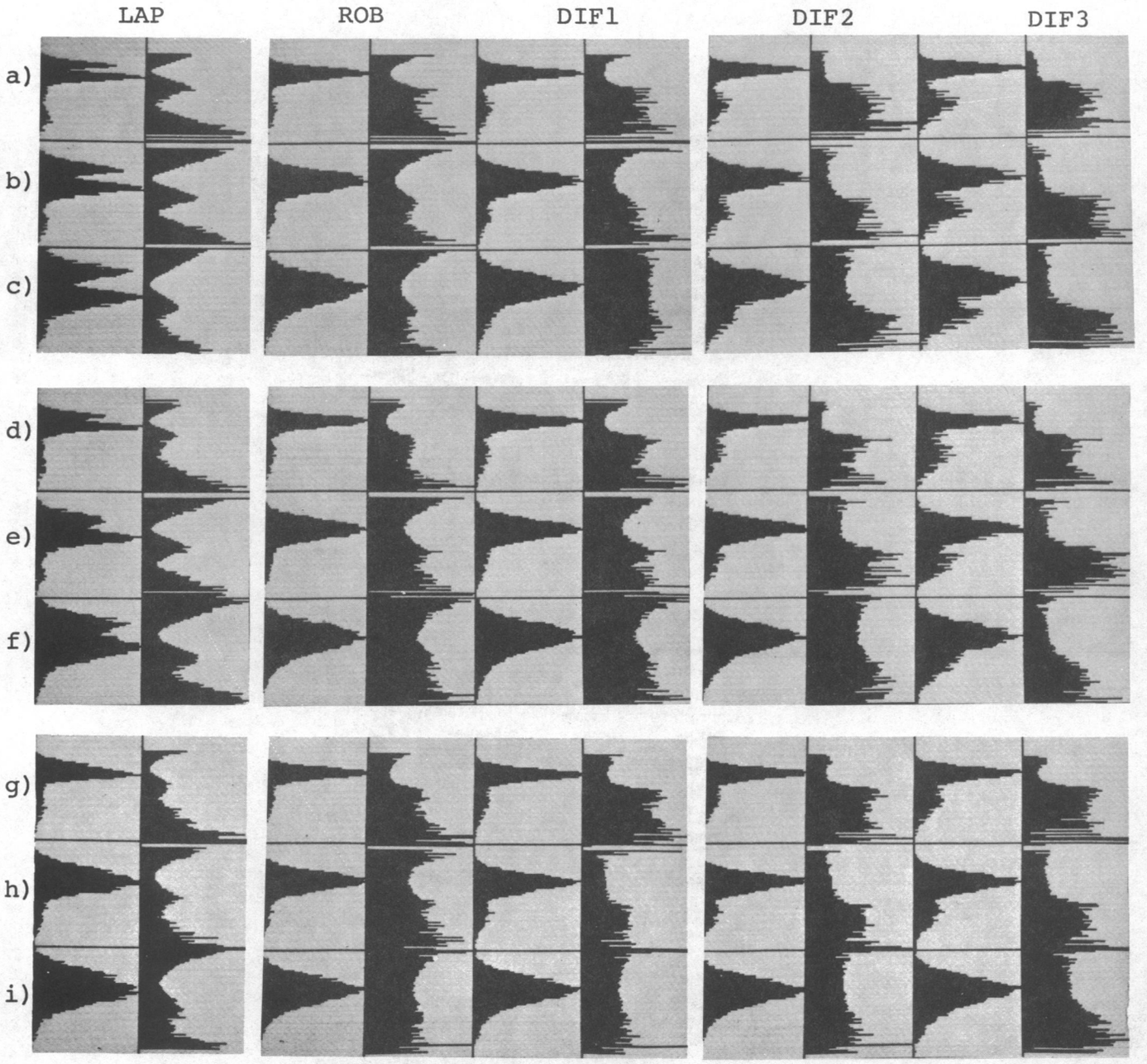

Fig. 16. Histograms for nine images in which points having high edge values are given higher weights, and results of dividing these histograms pointwise by unweighted histograms.

ACKNOWLEDGMENT

The help of Ms. Shelly Rowe in preparing this paper is gratefully acknowledged.

REFERENCES

[1] A. Rosenfeld and A. C. Kak, *Digital Picture Processing.* New York: Academic, 1976, sec. 8.1.

[2] J. M. S. Prewitt and M. L. Mendelsohn, "The analysis of cell images," *Annals N.Y. Acad. Sci. 128*, pp. 1031–1053, 1966.

[3] D. P. Panda and A. Rosenfeld, "Image segmentation by pixel classification in (gray level, gradient) space," *IEEE Trans. Comput.*, vol. 27, pp. 875–879, 1978. See also D. P. Panda, "Segmentation of FLIR images by pixel classification," Univ. of Maryland Computer Science Center Tech. Rep. 508, 1977.

[4] D. Mason, *et al.*, "Measurement of *C*-bands in human chromosomes" (preprint).

[5] J. S. Weszka and A. Rosenfeld, "Threshold selection, 4," Univ. of Maryland Computer Science Center Tech. Rep. 336, 1974.

[6] Y. H. Katz, "Pattern recognition of meteorological satellite cloud photography," *Proc. 3rd Symp. on Remote Sensing of Environment*, Institute of Science and Technology, Univ. of Michigan, 1965, pp. 173–214.

[7] J. S. Weszka and A. Rosenfeld, "Threshold selection techniques, 5," Univ. of Maryland Computer Science Center Tech. Rep. 349, 1975.

[8] J. S. Weszka, R. N. Nagel, and A. Rosenfeld, "A threshold selection technique," *IEEE Trans. Comput.*, vol. 23, pp. 1322–1326, 1974. See also idem., "A technique for facilitating threshold selection for object extraction from digital pictures," Univ. of Maryland Computer Science Center Tech. Rep. 243, 1973.

[9] S. Watanabe and CYBEST group, "An automated apparatus for cancer prescreening: CYBEST," *Comput. Graphics Image Proc. 3*, pp. 350–358, 1974.

[10] J. S. Weszka, J. A. Verson, and A. Rosenfeld, "Threshold selection techniques, 2," Univ. of Maryland Computer Science Center Tech. Rep. 260, 1973.